Catalysis Letters (2021) 151:548–558
https://doi.org/10.1007/s10562-020-03304-x

Calix[4]pyrrole Stabilized PdNPs as an Efficient Heterogeneous Catalyst for Enhanced Degradation of Water-Soluble Carcinogenic Azo Dyes

Anita Kongor[1] · Manthan Panchal[1] · Mohd Athar[2] · Manoj Vora[1] · Bharat Makwana[3] · P. C. Jha[4] · Vinod Jain[1]

Received: 21 August 2019 / Accepted: 29 June 2020 / Published online: 6 July 2020

Abstract

One-pot synthesis of palladium nanoparticles (PdNPs) has been achieved using calix[4]pyrrole hydrazide (MCPTH) as both reducing as well as capping agent. The synthetic procedure involves the use of environmentally benign water as solvent media. MCPTH-PdNPs have been characterized by using various analytical techniques. Transmission electron microscope analysis visualized the presence of well-dispersed and spherical Pd nanoparticles with an average dimension of 3–4 nm. Powder X-ray diffraction pattern portrayed the presence of face-centered cubic crystal structured PdNPs. A zeta potential value of − 26.2 mV suggests better stability of the nanoparticles. The heterogeneous catalytic activity of MCPTH-PdNPs was studied by probing the reduction of two carcinogenic azo dyes, namely, methylene blue and methyl orange in the presence of sodium borohydride. A remedial pathway for the process of dye degradation is proposed where the catalytic activity of Pd is faciled by the transfer of electrons from MCPTH to the metal centre. The mechanism for dye degradation is further substantiated by Density Functional Theory (DFT) calculations. The results of this work provide not only insight into fabrication of nanoparticles using calixarene platforms but also open new vistas to environmental remediation.

Electronic supplementary material The online version of this article (https://doi.org/10.1007/s10562-020-03304-x) contains supplementary material, which is available to authorized users.

✉ Vinod Jain
drvkjain@hotmail.com

[1] Department of Chemistry, School of Sciences, Gujarat University, Navrangpura, Ahmedabad, Gujarat 380009, India

[2] School of Chemical Sciences, Central University of Gujarat, Sector-30, Gandhinagar 382030, India

[3] Department of Chemistry, HVHP Institute of Post Graduate Studies and Research, Kadi Sarva Vishwavidyalaya, Gandhinagar, Gujarat 382715, India

[4] Centre for Applied Chemistry, Central University of Gujarat, Sector-30, Gandhinagar 382030, India

Graphic Abstract

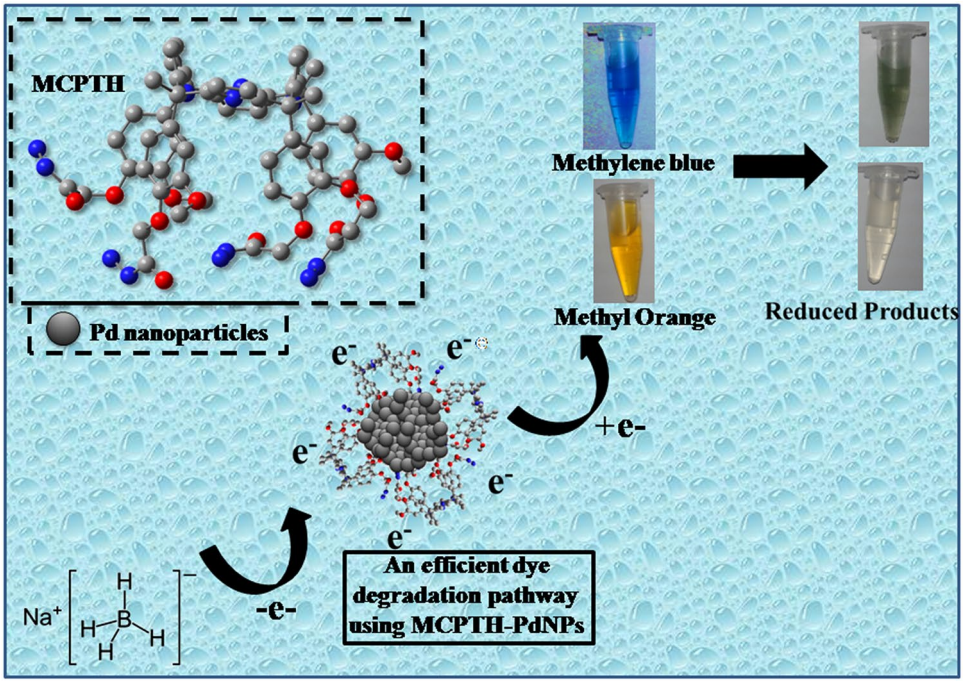

Keywords Palladium nanoparticles · Calix[4]pyrrole · Heterogeneous catalyst · Carcinogenic dyes · Methylene blue · Methyl orange

1 Introduction

The extensive use of azo dyes in various industrial processes and their inadequate discharge into water bodies has become a major concern among environmental chemists [1, 2]. Most of these wastewaters are found to contain considerable amounts of azo dyes and their degraded products, which are highly carcinogenic [3, 4]. The low degradability of some synthetic and toxic dyes causes them to enter the food chain via fertilizers used from sewage sludge [5, 6]. Also, these coloured effluents can be mixed with surface and ground water systems that get transferred to drinking water causing allergies, skin irritation, cancer and mutations [7]. The dissemination of coloured wastewaters in the ecosystem is a source of aesthetic pollution, eutrophication, and perturbations in aquatic life [8]. Among various azo dyes, methylene blue and methyl orange are most commonly used in textile and food industries as colouring agents [9]. These dyes are thought to be harmful due to their adverse health issues in living systems such as, skin eczema and intestinal cancer on ingestion [10, 11]. Unfortunately, the degradation of such organic dyes to non-toxic products is difficult as they are highly stable and resistant to microbiological attack [12–14]. Numerous methodologies based on physicochemical techniques, biological treatments, chemical methods such as ozonation and advanced oxidation processes using Fenton's reagent have been developed to treat dye effluents [15]. However, the downside of using these methods includes expensive cost of equipments, operational problems, inefficiency, and need of large land area for biological treatment. To circumvent these problems, a growing interest has been raised for efficient degradation of dyes using simple materials facilitating quick response.

Among metal nanoparticles, palladium nanoparticles (PdNPs) have recently gained attention as eco-friendly catalytic systems for Suzuki–Miyaura [16], oxidation of functionalized alcohols [17], hydrogenation and Heck coupling reactions [18]. The catalytic property of nanoparticles is due to its high surface energy which usually results in its aggregation during the course of its catalytic function [19, 20]. Thus, to achieve high activity and durable applicability, many different stabilizing agents have been used for preparing nanoparticles [21–24].

The full contact of nanoparticles in the superstructures with their external surroundings is important for enhancing the catalytic efficiency [25]. Accordingly, in comparison to conventional superstructures, the enveloping of nanoparticles with macrocyclic structures possessing inherent hollow cavity is believed to increase the surface contact of nanoparticles with their surroundings which thereby

increases the catalytic response. Eventually, the synthesis and application of palladium nanoparticles functionalized with different macrocyclic structures involving calixarenes have recently been at the forefront of research due to their tremendous range of applications [26–35]. Thus, it is desirable to develop metal nanoparticles based on functionalized calixarenes with many potential applications [36]. Recently, the use of new self-assembled material based on 4-sulfocalix[4]arene and ruthenium nanoparticles has been reported for reduction of Brilliant Yellow azo dye in the presence of hydrazine hydrate [37]. In the recent times, different research groups have achieved success in the synthesis of palladium nanoparticles using laser ablation methods for fabrication of palladium nanoparticles and used it for catalytic dye degradation applications [38]. Chen et al. reported the catalytic properties of lignin-based phenolic nanosphere supported palladium nanoparticles prepared by hydrothermal synthesis [39]. Although having good catalytic capacity, these methods involve long procedural steps to synthesize nanoparticles, thus, there are increasing interests to use alternative methods such as one-pot chemical reduction method for the synthesis of palladium nanoparticles. The present work demonstrates the efficient use of calix[4]pyrrole tetrahydrazide derivative (MCPTH) [24] as both reducing agent and stabilizer for the synthesis of palladium nanoparticles and its application as heterogeneous catalyst. However, to the best of our knowledge, the advantageous use of calix[4]pyrrole based nanoparticles for azo dye degradation is unprecedented. MCPTH-PdNPs efficiently reduces two carcinogenic azo dyes, namely, methylene blue and methyl orange in the presence of $NaBH_4$. MCPTH-PdNPs exhibits good water dispersibility, stability, high catalytic activity, and efficient recycling ability. The experimental results were also substantiated using the theoretical insights such as Density Functional Theory (DFT) and Molecular Dynamics (MD) simulations.

2 Experimental Work

2.1 Materials and Methods

Palladium acetate, methylene blue (MB) and methyl orange (MO) were purchased from Sigma-Aldrich (Mumbai, India) and used as received. All other chemicals and solvents were obtained from commercial sources and were used as received without further purification.

2.2 Synthesis of MCPTH-PdNPs

MCPTH-PdNPs were successfully prepared via simple one-pot chemical reduction process using MCPTH as both reducing and capping agent (Scheme 1). The synthetic procedure (Scheme S1) and the spectroscopic characterization of calix[4]pyrrole derivatives has been mentioned in the supporting information (Fig. S1–S11). Hydrazide derivative of calix[4]pyrrole platform, MCPTH [24] (0.001 M in 100-mL water) was added to the boiling solution of palladium acetate (0.001 M in 100-mL water). The reaction mixture was heated at constant temperature (80 °C) controlled by water bath. After 15 min, the colour of the mixture changed from brownish yellow to colloidal black confirming the formation of PdNPs. The functionalization of MCPTH on the surface of palladium nanoparticles (PdNPs) takes place in two steps. First, the hydrazide group reduces the Pd^{2+} ions to metallic Pd^0 which further nucleates to form PdNPs. Second, the macrocyclic ligand (MCPTH) restrains the growth of the palladium nanoparticles by stabilizing/capping it in the hollow cavity in an effective manner to prevent its aggregation. The MCPTH ligand stabilizes the nanoparticles through efficient capping/attachment/functionalization due to its web type architecture.

2.3 Characterization

UV–Vis spectra were recorded on Jasco V-570 UV–Vis recording spectrophotometer (Tokyo, Japan) using quartz cuvette. High-resolution transmission electron microscopy (HR-TEM) was analyzed on a JEOL JEM 2100 microscope operating at an accelerated voltage of 200 kV. Powder X-ray diffraction (XRD) was recorded on a PANalytical Empyrean powder diffractometer using Cu Kα. Inductively Coupled Plasma-Atomic Emission Spectrometer (ICP-AES) JY 2000-2 model was used to check the absence of Pd in supernatant liquid collected after centrifugation. Dynamic light scattering (DLS) measurements were operated with a Zetasizer NanoZS (Malvern Instruments). Fourier transform infra-red (FTIR) spectra of the synthesized palladium nanoparticles were recorded at room temperature on Bruker, Tensor 27 Infrared spectrometer. Nanoparticle tracking analysis (NTA) was determined using NanoSight NS300 (Malvern Instruments, Worcestershire, UK) equipped with a green laser (532 nm), a scientific complementary metal–oxide–semiconductor (CMOS) camera and NanoSight software version 3.2 Build 3.2.16.

2.4 Degradation Studies

0.5 mL of freshly prepared $NaBH_4$ solution (100 mM) was added to 2 mL of aqueous methylene blue and methyl orange solution (0.1 mM), respectively under stirring conditions. Subsequently, 5.0 mg of MCPTH-PdNPs was added to the solution mixture. The experiments were carried out into a standard 1-cm path-length quartz cell keeping the stirring speed 80 rpm. To optimize the catalytic reaction, the completion time for the reduction reaction using different

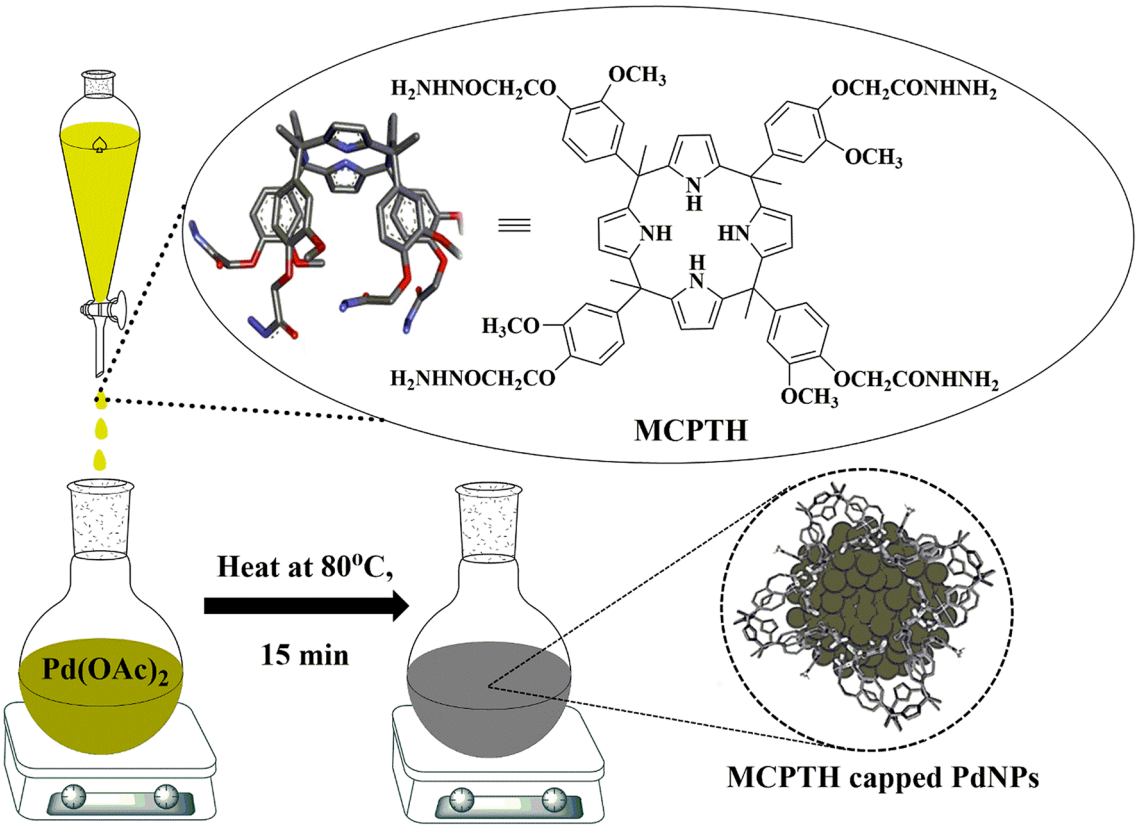

Scheme 1 Schematic representation for the synthesis of MCPTH-PdNPs

amount of MCPTH-PdNPs was evaluated. The highest conversion was obtained when 5.0 mg of MCPTH-PdNPs was used. However, on further increasing the amount of catalyst, no decrease in reduction time was observed. The degradation efficiency of both the dyes was calculated as degradation efficiency (%) = $100(C_0-C)/C_0$, where C_0 is the initial dye concentration, and C is the dye concentration in the solution at a given time.

3 Results and Discussion

3.1 Characterization of MCPTH-PdNPs

UV–Vis spectra was measured to ensure the complete reduction of Pd(II) ions to Pd(0) ions. The colloidal palladium nanoparticles do not have a SPR peak in the visible region [40]. As can be seen from Fig. 1, the UV–Vis spectrum of palladium acetate shows absorption maximum at around 400 nm, which is characteristic of Pd(II) ions [25]. After reaction with MCPTH, the peak observed at 400 nm disappeared, indicating the complete conversion of Pd(II) to Pd(0) nanoparticles. Additionally, all the MCPTH molecules after the reduction process, effectively caps the Pd(0) nanoparticles which was evidenced by the absence of absorbance peak due to MCPTH. This also confirms the absence of any unreacted MCPTH in the centrifugate of MCPTH-PdNPs solution. The inset of Fig. 1 shows the UV–Vis spectra of MCPTH and re-dispersed MCPTH-PdNPs which notions the efficiency of MCPTH as both reducing as well as stabilizing agent. This results were in accord with our previous studies [41, 42].

The size and morphology of MCPTH-PdNPs were further visualized using TEM analysis (Fig. 2a). The TEM images have shown the presence of well-dispersed and spherical Pd nanoparticles with an average dimension of 3–4 nm. Figure 2b displays HR-TEM image with well-defined clear lattice fringes. The inter-planar spacing "d" value is measured to be 0.221 nm, which corresponds to the lattice plane of (111) with the face-centered cubic phase of the Pd. Figure 2c shows selected area electron diffraction (SAED) pattern of MCPTH-PdNPs. The presence of four concentric ring patterns with intense spots evidenced the crystalline characteristic of the nanoparticles.

The X-ray diffraction (XRD) pattern reveals well-defined peaks at 2Θ values of 39.96°, 46.43°, 68.16° and 81.92° corresponding to (111), (200) (220) and (311) planes of the face centered cubic (*fcc*) structured palladium (JCPDS No.

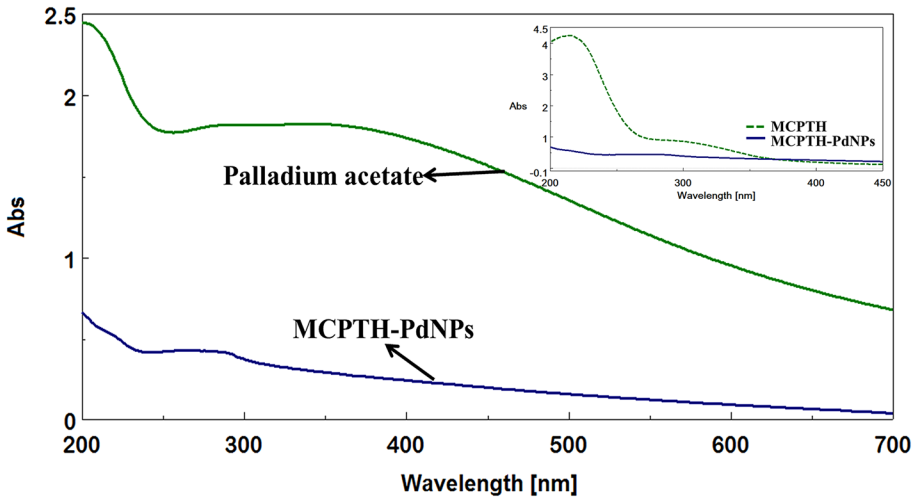

Fig. 1 UV–Vis spectrum of MCPTH-PdNPs. Inset shows the absence of peaks (220 and broad peak around 300 nm) due to MCPTH

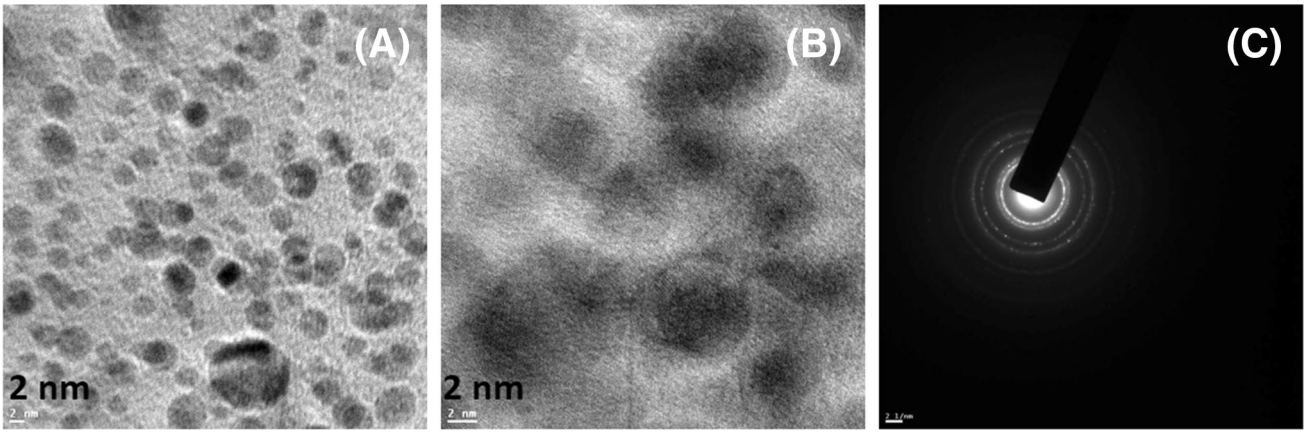

Fig. 2 **a** TEM **b** HR-TEM **c** SAED of MCPTH-PdNPs

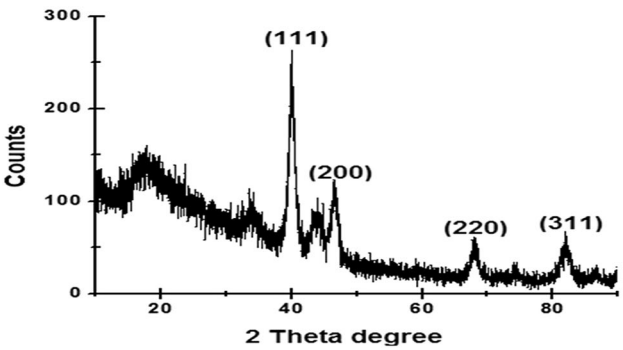

Fig. 3 XRD of MCPTH-PdNPs

46-1043), respectively [43] (Fig. 3). The application of the Debye–Scherrer formula to the strongest diffraction peaks for Pd (111) gives a crystallite size of 4.3 nm which falls in line with the TEM results. The presence of additional broad peak, 2Θ value between 18 and 20° has been ascribed to the capping compound [44], illustrating that the calix[4] pyrrole units were introduced onto the surface of palladium nanoparticles.

The FT-IR spectrum of MCPTH-PdNPs was carried out to investigate the interactions of MCPTH on the surface of palladium nanoparticles (Fig. S12). The broad peaks observed at 3238.50 cm^{-1} and 1669.76 cm^{-1} are assigned to –NH and –CONH groups of MCPTH, respectively. The results confirms that the reduction of palladium ions and the stabilization of the palladium nanoparticles is due to the functional groups present in MCPTH [24]. A zeta potential value of – 26.2 mV indicates that the palladium nanocatalyst is sufficiently coated with negatively charged MCPTH molecules which kept the synthesized PdNPs stable more than 90 days. This reveals that the synthesized MCPTH-PdNPs are highly stable due to strong inter-particle electrostatic repulsion of surface capped MCPTH (Fig. 4a).

The size distribution graph of MCPTH-PdNPs nanoparticles was estimated by dynamic light scattering

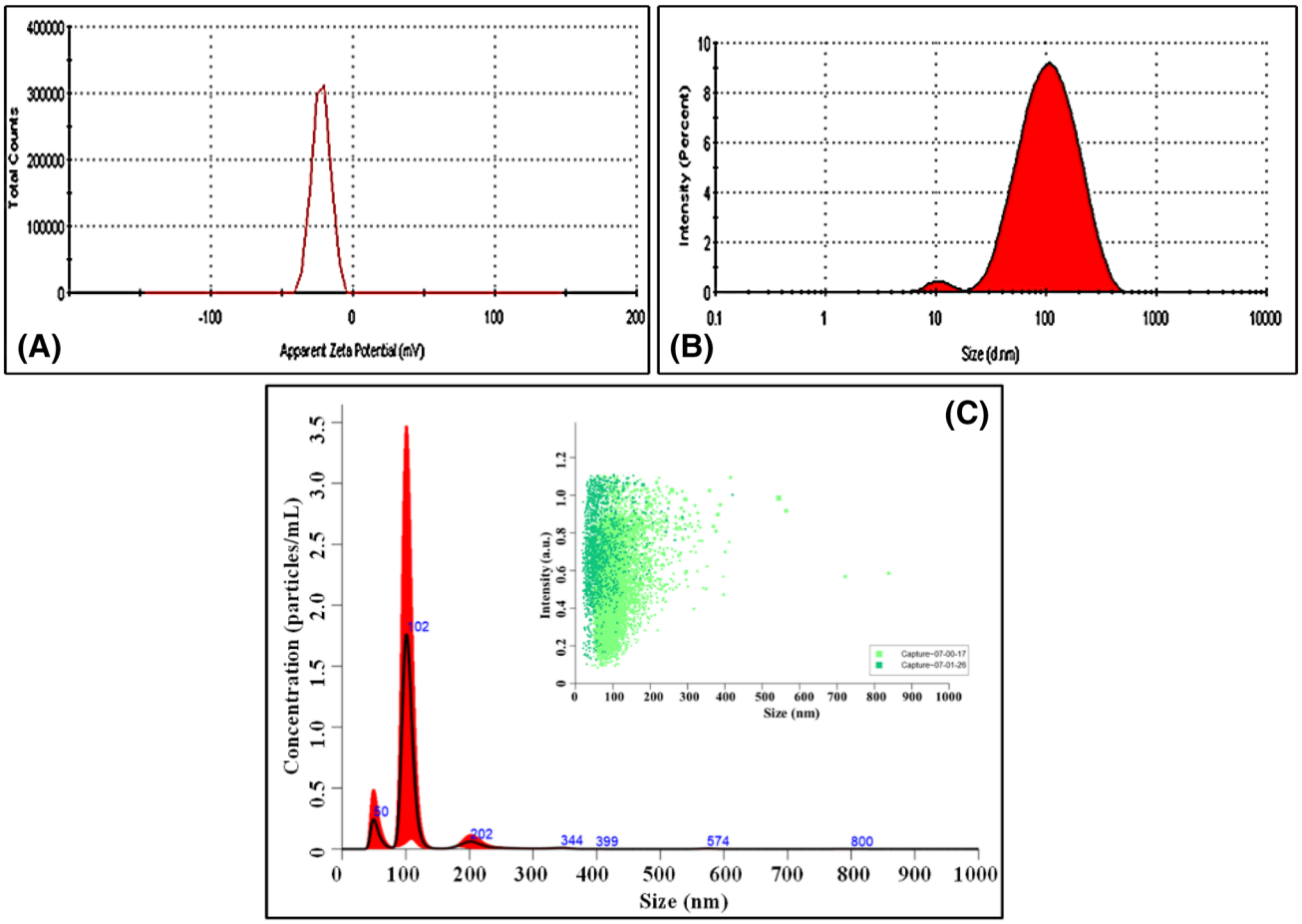

Fig. 4 **a** Zeta potential **b** Size distribution graph of MCPTH-PdNPs by DLS **c** Size distribution plot: mean (109.9 nm), mode (101.0 nm) and SD (50.2 nm) by NTA

experiments under optimal conditions is shown in Fig. 4b. The DLS pattern illustrates zeta average diameter (d.nm) of 86.05 nm with polydispersity index (PdI) of 0.36. Nanoparticle tracking analysis is an innovative system to determine the size mode distribution of particles with respect to particle number [45, 46]. Both DLS and NTA can be used as complementary methods as because DLS measures average size of the particles based on scattered light intensity whereas in case of NTA, the mean size is measured based on number distribution. However, NTA also provides particle-number concentration and hydrodynamic-size distributions which supports the notion of interactions of nanoparticles with the surrounding organic moieties. The MCPTH capped nanoparticles showed a concentration of $(4.20 \pm 3.17) \times 10^9$ particles/mL (Fig. 4c). The inset of Fig. 4c also shows the individual particle scattered light intensity (a.u) vs. size of MCPTH capped PdNPs.

3.2 Catalytic Degradation of MB and MO Using MCPTH-PdNPs

With the development of modern industries, the discharge of azo dyes into water bodies as industrial waste is considered to be highly carcinogenic to aquatic environment and to human health as well. Current efforts are being made to meet the challenge of developing such catalysts which are water dispersible and can be easily separable or recycled from water. The practical use of various fabricated nanoparticles as heterogeneous catalysts possessing increased surface area is expected to solve this problem. Many researchers have reported the use of fabricated palladium nanoparticles as an efficient and stable catalyst for dye degradation under ambient temperature conditions [47–49].

In the process of azo dye degradation, electrons released from reduced compounds such as, carbohydrates [50], fatty acids [51], bacteria and enzymes [52, 53] play an important

role to mediate the reduction reaction. Herein, the catalytic efficiency of MCPTH-PdNPs in the reduction of MB and MO has been investigated using $NaBH_4$ as an effective electron donor. Figure 5a displays the UV–Visible absorption spectra of degradation of MB by $NaBH_4$ in the absence and presence of MCPTH-PdNPs, respectively. The absorption peak (λ_{max}) of MB at 664 nm with a shoulder peak at 612 nm which corresponds to the conjugated structure linked by the azo band (N = N) in the MB molecule. After catalytic degradation the main characteristic peak centred at 664 nm decreased markedly with time and, the peak disappears nearly after 15 min of reaction time. At the same time, after 15 min the colour changed from blue to colourless, which suggested the complete degradation of MB (inset of Fig. 5b). However, in the absence of MCPTH-PdNPs, no any colour change or observable degradation was observed. In the present study, no re-oxidation of the reduced methylene blue was observed. In case of MO, the absorption peak (λ_{max}) at 463 nm originates from a conjugated structure formed by the azo bond under the strong influence of the electron-donating dimethyl amino group. Figure 5d, e displays the UV–Visible absorption spectra of degradation of methyl orange by $NaBH_4$ in the absence and presence of MCPTH-PdNPs, respectively. It was observed that the intensity of main characteristic peak centred at 463 nm decreased markedly and nearly disappeared after reduction time of 12 min. Nevertheless, the absorption intensity at 463 nm remained unaltered in the absence of MCPTH-PdNPs. In this case also, $NaBH_4$ alone was not able to reduce the azo bond in the MO molecules. Therefore, it is reasonable to speculate that the heterogeneous catalytic system of MCPTH-PdNPs accelerates the degradation of both MB and MO. The percentage of degradation efficiency for MB and MO was calculated as 90.07% and 95.07% respectively.

The catalytic effect was further evaluated by the kinetics of the catalytic dye degradation reaction process with respect to MB and MO. It was rational to assume that the amount of sodium borohydride was much larger than that of the dyes; its concentration remained constant throughout the reaction. Hence, the reactions may be considered to follow pseudo-first order kinetics and the rate equation may be written as $\ln(C/Co) = -K_t$, where, K = pseudo-first order rate constant and was calculated directly from the slope of the straight line, Co = initial concentration of the dye and C = concentration at 't' time. The concentrations of MB and MO (C at time t) to their initial value C_0 (t = 0) were directly determined by the ratio of their respective absorbance, A_t/A_0 (A_0at 664 nm for MB and 463 nm for MO). The rate constant for the reduction of MB (Fig. 5c) and MO (Fig. 5f) was calculated from the slope of the linear plot and found to be 5.72×10^{-2} min^{-1} and 0.2047 min^{-1} respectively. The rate constant investigated in the present study is comparable

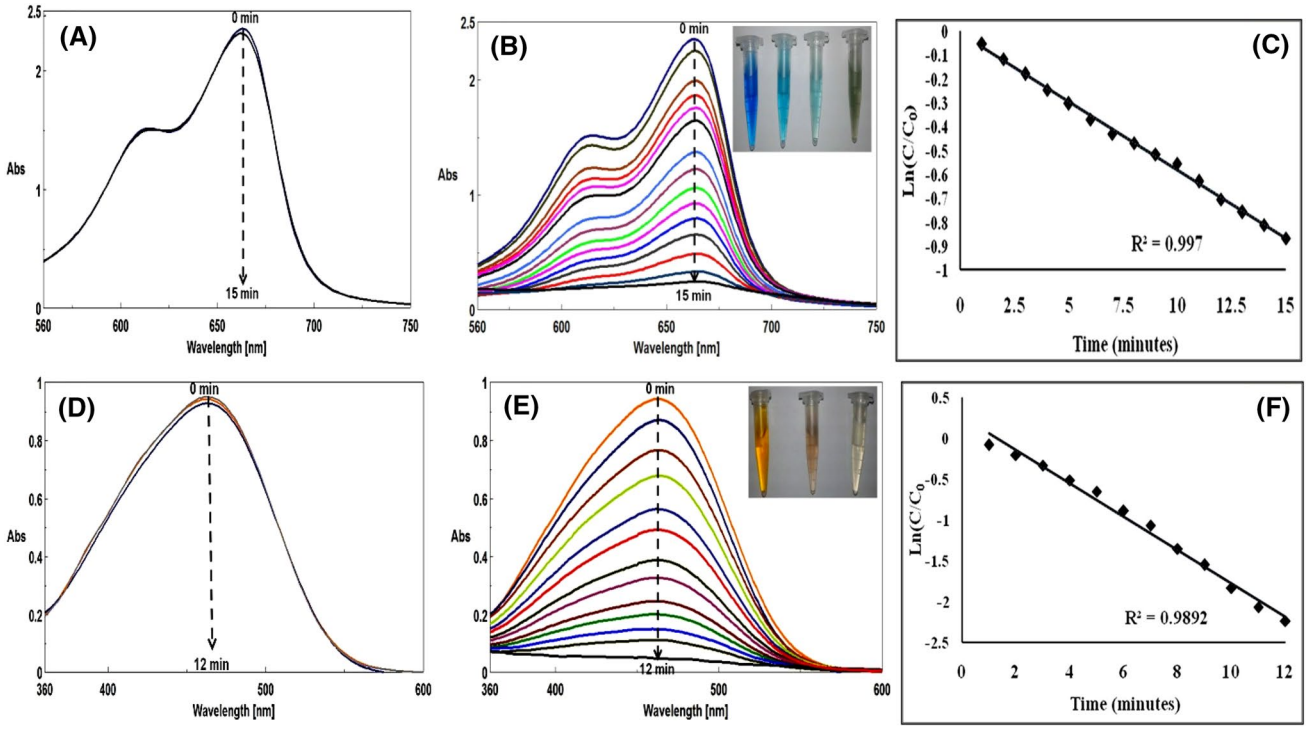

Fig. 5 UV–Visible absorption spectra of degradation of **a**, **b** MB and **d**, **e** MO by NaBH4 in the absence and presence of MCPTH-PdNPs, respectively (**c**–**f**). The pseudo-first order linear plot of $\ln(C/C_0)$ vs. time of MB and MO, respectively

with previous reports [54, 55]. The results obtained in the present work have been compared to other palladium based catalyst as shown in Table S1. The catalytic activity of the studied nanocatalyst was efficient and comparable with other reported palladium based catalyst. Previously, Hong et al. reported that the adsorption abilities for dyes were favorably influenced by calixarene modified multi-walled carbon nanotubes (MWCNTs) when compared to unmodified hydroxyl MWCNTs [56]. There was no any substantiate change in the degradation results for both the azo dyes, MB and MO in the presence of MCPTH alone (Fig. S13 a–d). Even in the case of PdNPs coated with citrate ligand, which was prepared according to reported procedure using $PdCl_2$ as starting material [57] showed very slight change in the absorption spectra, which may be due to the fact that citrate bound PdNPs exhibited electrostatic repulsion to borohydride ions which discouraged any catalytic activity. The degradation studies were also compared with other cationic (methyl violet) and anionic (Eosin Y and Congo red) dyes by observing their UV–Visible spectra (Fig. S14 a–c). It has been understood that, the degradation process was very slow and inefficient. According to previous studies, the reason behind less facile degradation process for various dyes has been reported due to (1) complex chemical structures which increases the steric hindrance [4, 58] (2) chemical structure of the dye molecules [59, 60] and (3) molecular size of the dye molecules [61]. Thus, in the present case also, the large molecular size as well as the chemical functionalities which hinders the physical contact of the dyes with PdNPs.

3.3 Proposed Mechanism for Dye Degradation

In the present work, the resulting calix-nano hybrid possesses a hydrophobic calix[4]pyrrole conjugate, a heterogeneous surface, and the capability to reduce [62]. This makes the palladium nanocatalyst stable and is useful for carrying out catalytic activity in water. Alternatively, the palladium nanoparticles stabilized by MCPTH functions as the electron mediator between borohydride ions (reductant) and azo dyes (oxidant), and the electron transfer process occurs via the surface of palladium nanoparticles. Eventually, the electrons released by borohydride ions are adsorbed on the surface of the palladium nanocatalyst and the dye molecules are reduced to respective hydrazide or aniline derivatives. The uptake of electrons by the azo dyes leads to easy degradation by an oxidation–reduction process. Hence, it is reasonable to speculate that during the catalytic reduction process, the azo band completely destroys and forms some degradation products. The formation of intermediates such as hydrazine and benzene derivatives have also been reported previously [53]. The formation of the degraded products obtained after the catalytic reaction of both methylene blue and methyl orange were analyzed using gas chromatography-mass spectroscopy method (GC–MS). The molecular structures of the possible reaction intermediates due to the fragmentation of methylene blue and methyl orange has been shown in Fig. 6. In case of MB, different intermediate products with m/z values of 229, 256, 270 and 94 were identified due to the cleavage of one or more methyl substituent on the amine groups [63]. In case of MO, the cleavage of azo bond, yielded 4-aminobenzenesulfonic acid and N, N'-dimethylaniline, aniline at m/z values of 173, 121 and 94 respectively. In addition, other fragment ions with the corresponding peaks of *N,N´*-dimethylbenzene diamine and benzene sulfonic acid were also engendered in the degradation process [64, 65]. The mass spectra recorded for MB and MO has been depicted in Fig. S15. To further shed light on the application of MCPTH-PdNPs for the azo dye degradation, Fig. S16 depicts a schematic representation for the catalytic mechanistic pathway.

To substantiate the experimental results, we have performed the natural bond orbital (NBO) analysis to determine the intramolecular donor–acceptor interactions and to find the electronic populations in hybrid orbitals (Fig. S17a, b). Results have shown that the hydrazide groups of MCPTH comprise higher NBO charges as well as Mulliken charges compare to Pd bound MCPTH. The HOMO in MCPTH-Pd is purely localized on the Pd centre which thereby enables the transfer of electrons to both the dyes (Fig. S17c, d). As a consequence, reduction of the dye takes place in close agreement with the NBO scheme and experimental findings.

3.4 Recyclability Study

The nanoparticles were separated by centrifugation, washed with mixture of water and acetone, dried in a vacuum oven, and then stored for the next cycle at ambient temperature. The palladium nanocatalyst showed good performance up to 6th cycle (79.2% for MB degradation and 80.7% for MO degradation), however, in the 7th consecutive catalytic run, the efficiency was reduced to 61.2% and 63.7% for MB and MO, respectively. The results are shown in Fig. 7. No significant loss of catalytic activity up to six subsequent cycles also indicates that the same proportions of palladium nanoparticles were used in all six catalytic runs. TEM analysis was carried out to investigate the morphology of the nanoparticles after sixth catalytic run. As shown in Fig. 8 a, b, highly aggregated lumps of the MCPTH-PdNPs was visualized which determined the decreased catalytic activity of the nanoparticles for degrading MB and MO, respectively. The turnover number for the heterogeneous system, MCPTH-PdNPs was calculated to be 2.36×10^{20} molecules per gram and 2.4×10^{20} molecules per gram for MB and MO, respectively. Intuitively, in case of calix reduced as well as capped nanoparticles system, it is difficult to speak about the catalyst concentrations, additionally, we found only a few publications that report turnover numbers/rates for a

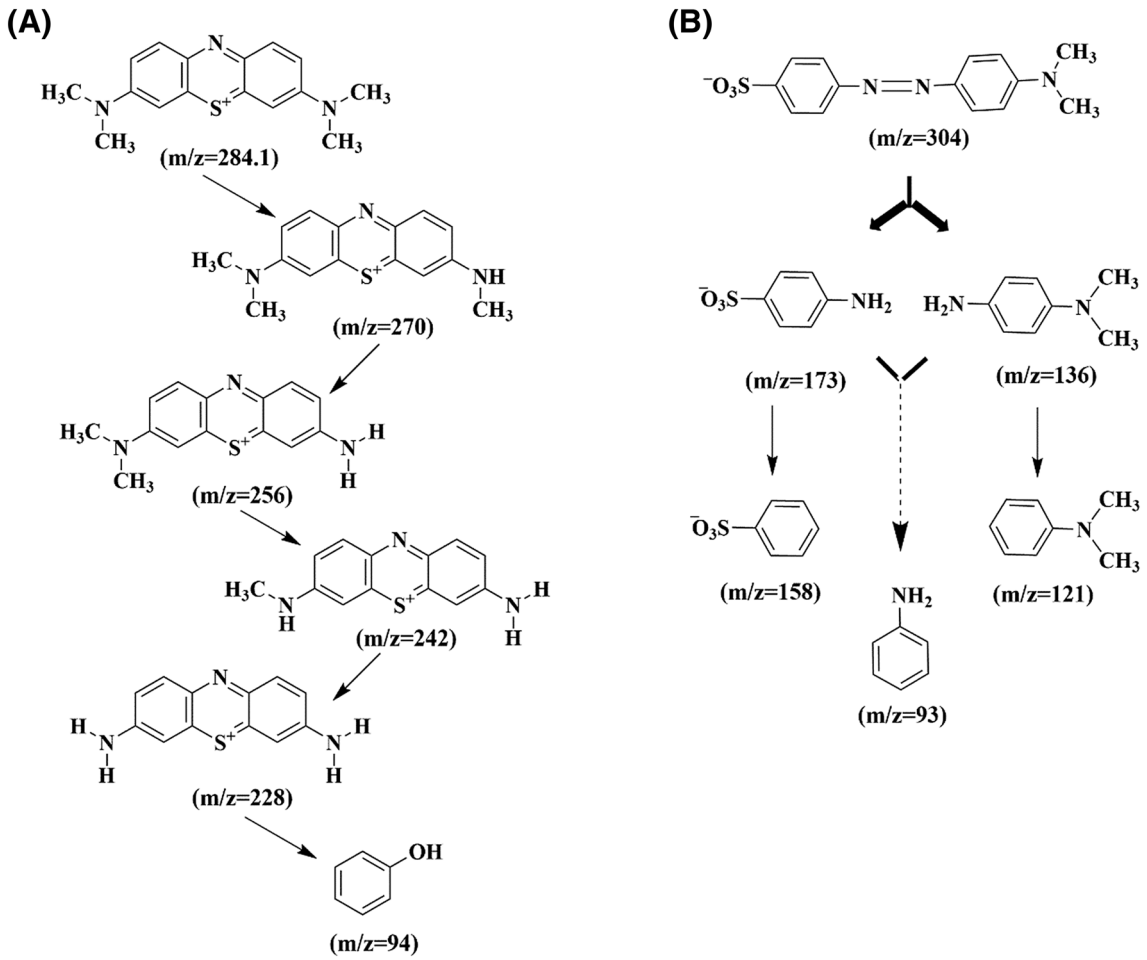

Fig. 6 Degradation pathway showing the intermediates formed after catalytic degradation of **a** methylene blue and **b** methyl orange

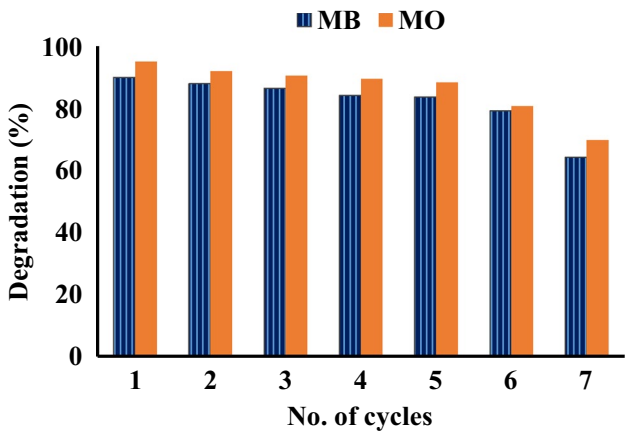

Fig. 7 Recycle ability of MCPTH-PdNPs for MB and MO catalytic degradation

given reaction and comparisons with other catalysts from the literature [62, 66].

4 Conclusion

In conclusion, a simple one-pot synthesis of palladium nanoparticles is reported using web-like calix[4]pyrrole tetrahydrazide (MCPTH) as both reductant and stabilizer. The nanoparticles are prepared in water with an average dimension of 3–4 nm and are quite stable. Further, the synthesized MCPTH-PdNPs have been used for the catalytic reduction of two azo dyes, methyl orange and methylene blue in water. The catalytic efficiency of the nanocatalyst was approximately stable for six subsequent cycles which makes them potential for applications pertaining to environmental remediation protection. Moreover, the present work demonstrates the applicability of other unprecedented nanoparticles based on calixarenes for the catalytic degradation of organic dyes in water.

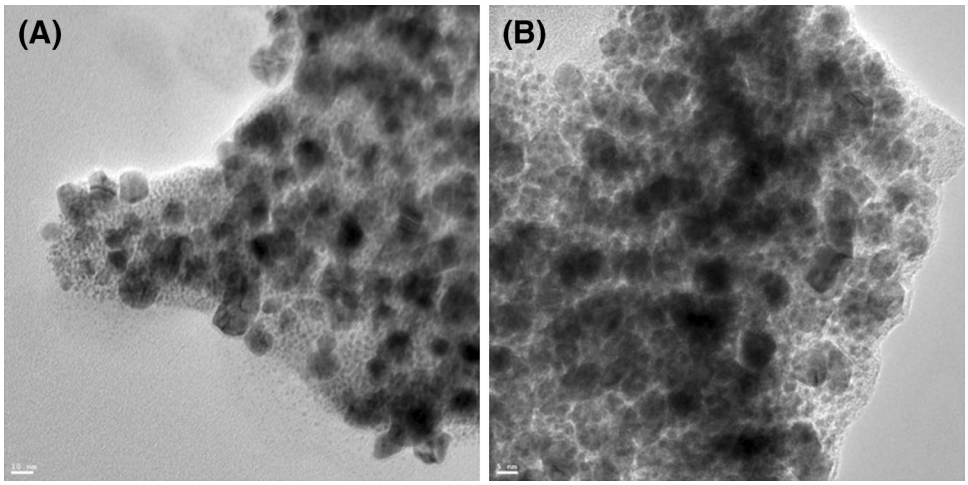

Fig. 8 TEM micrographs of MCPTH-PdNPs **a** for degradation of MB and **b** MO after sixth cycle

Acknowledgements The authors thank the financial assistance provided by DST-SERB, New Delhi through the project scheme SERB REF. No EMR/2016/001958. V. K. Jain would like to acknowledge UGC-Mid Career Award for financial assistance (19-213/2018-BSR). Anita Kongor gratefully acknowledge the financial assistance provided by Department of Science & Technology (DST)—Innovation in Science Pursuit for Inspired Research (INSPIRE), (New Delhi). Manoj Vora gratefully acknowledges the financial support received from UGC in the form of Rajiv Gandhi National Fellowship, RGNF-JRF. Manthan K. Panchal gratefully acknowledges Human Resource Development Group—Council of Scientific & Industrial Research (CSIR), New Delhi for Research Associateship Fellowship (File No. 09/70 (0064) 2K19 EMR-I). The authors also acknowledge Central Salt & Marine Chemicals Research Institute (Bhavnagar), Oxygen Healthcare-Ahmedabad (O2h), Sophisticated Analytical Instrument Facility (Panjab University) and Gujarat Forensic Sciences University (Gandhinagar), for providing instrumental facilities and UGC Infonet & Information and Library Network (INFLIBNET) (Ahmedabad) for e-journals.

References

1. Jiao T, Guo H, Zhang Q, Peng Q, Tang Y, Yan X, Li B (2015) Sci Rep 5:srep11873
2. Rauf M, Ashraf SS (2009) Chem Eng J 151(1):10–18
3. Brown MA, De Vito SC (1993) Crit Rev Environ Sci Technol 23(3):249–324
4. Zhang X, Lin M, Lin X, Zhang C, Wei H, Zhang H, Yang B (2014) ACS Appl Mater Interfaces 6(1):450–458
5. Petrović M, Barceló D (2000) Anal Chem 72(19):4560–4567
6. Webber M, Rogers H, Watts C, Boxall A, Davis R, Scoffin R (1996) Sci Total Environ 185(1–3):27–44
7. Acemioğlu B (2004) J Colloid Interface Sci 274(2):371–379
8. Lachheb H, Puzenat E, Houas A, Ksibi M, Elaloui E, Guillard C, Herrmann J-M (2002) Appl Catal B 39(1):75–90
9. Dutta DP, Rathore A, Ballal A, Tyagi A (2015) RSC Adv 5(115):94866–94878
10. Chung K-T, Stevens SE, Cerniglia CE (1992) Crit Rev Microbiol 18(3):175–190
11. Stradling B, Aranha G, Gabram S (2002) Am J Surg 184(4):350–352
12. Lefebvre O, Moletta R (2006) Water Res 40(20):3671–3682
13. Mohmood I, Lopes CB, Lopes I, Ahmad I, Duarte AC, Pereira E (2013) Environ Sci Pollut Res 20(3):1239–1260
14. Forgacs E, Cserhati T, Oros G (2004) Environ Int 30(7):953–971
15. Shi X, Tian A, You J, Yang H, Wang Y, Xue X (2018) J Hazard Mater 353:182
16. Faria VW, Oliveira DG, Kurz MH, Gonçalves FF, Scheeren CW, Rosa GR (2014) RSC Adv 4(26):13446–13452
17. Mifsud M, Parkhomenko KV, Arends IW, Sheldon RA (2010) Tetrahedron 66(5):1040–1044
18. Cirtiu CM, Dunlop-Briere AF, Moores A (2011) Green Chem 13(2):288–291
19. Narayanan R, El-Sayed MA (2005) ACS Publ 109(26):12663–12676
20. Sun T, Zhang Z, Xiao J, Chen C, Xiao F, Wang S, Liu Y (2013) Sci Rep 3:2527
21. Wu M-L, Chen D-H, Huang T-C (2001) Langmuir 17(13):3877–3883
22. Dhakshinamoorthy A, Garcia H (2012) Chem Soc Rev 41(15):5262–5284
23. Grubbs RB (2007) Polym Rev 47(2):197–215
24. Makwana BA, Darjee S, Jain VK, Kongor A, Sindhav G, Rao MV (2017) Sens Actuators B 246:686–695
25. Zhang X, Lin M, Lin X, Zhang C, Wei H, Zhang H, Yang B (2013) ACS Appl Mater Interfaces 6(1):450–458
26. Yasin FM, Boulos RA, Hong BY, Cornejo A, Iyer KS, Gao L, Chua HT, Raston CL (2012) Chem Commun 48(81):10102–10104
27. Chen X, Yasin FM, Eggers PK, Boulos RA, Duan X, Lamb RN, Iyer KS, Raston CL (2013) RSC Adv 3(10):3213–3217
28. Chen X, Zang W, Vimalanathan K, Iyer KS, Raston CL (2013) Chem Commun 49(12):1160–1162
29. Kongor A, Panchal M, Mehta V, Bhatt K, Bhagat D, Tipre D, Jain VK (2016) Arab J Chem 10(8):1125–1135
30. Mehta V, Panchal M, Kongor A, Panchal U, Jain V (2016) Catal Lett 146(8):1581–1590
31. Panchal M, Kongor A, Mehta V, Vora M, Bhatt K, Jain V (2017) J Saudi Chem Soc 22(5):558–568
32. Yanilkin V, Nastapova N, Sultanova E, Nasretdinova G, Mukhitova R, Ziganshina AY, Nizameev I, Kadirov M (2016) Russ Chem Bull 65(1):125–132
33. Zang W, Chen X, Boulos RA, Toster J, Raston CL (2014) Chem Commun 50(96):15167–15170
34. Yasin FM, Iyer KS, Raston CL (2013) New J Chem 37(10):3289–3293
35. Sattler KD (2019) 21st Century nanoscience–a handbook: design strategies for synthesis and fabrication, vol 2. CRC Press, Boca Raton
36. Kongor AR, Mehta VA, Modi KM, Panchal MK, Dey SA, Panchal US, Jain VK (2016) Top Curr Chem 374(3):1–46

37. Rambabu D, Pradeep CP, Dhir A (2016) J Nanoparticle Res 18(12):381
38. Jaleh B, Karami S, Sajjadi M, Mohazzab BF, Azizian S, Nasrollahzadeh M, Varma RS (2020) Chemosphere 246:125755
39. Chen S, Wang G, Sui W, Parvez AM, Dai L, Si C (2020) Ind Crops Prod 145:112164
40. Creighton JA, Eadon DG (1991) Faraday Transac 87(24):3881–3891
41. Modi K, Patel C, Panchal U, Liska A, Kongor A, Jiri L, Jain V (2019) New J Chem 43(14):5611–5622
42. Kongor A, Panchal M, Athar M, Makwana B, Sindhav G, Jha P, Jain V (2018) J Photochem Photobiol A 364:801–810
43. Comisso N, Mengoli G (2003) Environ Chem Lett 1(4):229–232
44. Vyas G, Bhatt S, Paul P (2019) ACS Omega 4(2):3860–3870
45. Kim A, Ng WB, Bernt W, Cho N-J (2019) Sci Rep 9(1):1–14
46. Filipe V, Hawe A, Jiskoot W (2010) Pharm Res 27(5):796–810
47. Li G, Li Y, Wang Z, Liu H (2017) Mater Chem Phys 187:133–140
48. Kora AJ, Rastogi L (2016) Ind Crop Prod 81:1–10
49. Li S, Li H, Liu J, Zhang H, Yang Y, Yang Z, Wang L, Wang B (2015) Dalton Transac 44(19):9193–9199
50. Sun J, Hu Y-y, Bi Z, Cao Y-q (2009) Biores. Technol 100(13):3185–3192
51. Van Der Zee FP, Bouwman RH, Strik DP, Lettinga G, Field JA (2001) Biotechnol Bioeng 75(6):691–701
52. Wesenberg D, Kyriakides I, Agathos SN (2003) Biotechnol Adv 22(1–2):161–187
53. Zimmermann T, Kulla HG, Leisinger T (1982) Eur J Biochem 129(1):197–203
54. Snoussi Y, Bastide S, Abderrabba M, Chehimi MM (2018) Ultrason Sonochem 41:551–561
55. Vilas V, Philip D, Mathew J (2016) Mater Chem Phys 170:1–11
56. Hong B, Wang W, Yang F (2015) Fuller Nanotub Carb Nanostruct 23(12):1077–1085
57. You J-G, Shanmugam C, Liu Y-W, Yu C-J, Tseng W-L (2017) J Hazad Mater 324:420–427
58. Azad UP, Ganesan V, Pal M (2011) J Nanoparticle Res 13(9):3951–3959
59. Fathinia M, Khataee A, Zarei M, Aber S (2010) J Mol Catal A 333(1–2):73–84
60. El Bekkali C, Bouyarmane H, Saoiabi S, El Karbane M, Rami A, Saoiabi A, Boujtita M, Laghzizil A (2016) J Adv Res 7(6):1009–1017
61. Gupta K, Khatri OP (2019) Chem Eng J 378:122218
62. Narkhede N, Uttam B, Rao CP (2019) ACS Omega 4(3):4908–4917
63. Yang C, Dong W, Cui G, Zhao Y, Shi X, Xia X, Tang B, Wang W (2017) RSC Adv 7(38):23699–23708
64. Shen T, Jiang C, Wang C, Sun J, Wang X, Li X (2015) RSC Adv 5(72):58704–58712
65. Jaafar NF, Jalil AA, Triwahyono S, Muhid MNM, Sapawe N, Satar MAH, Asaari H (2012) Chem Eng J 191:112–122
66. Genorio B, Strmcnik D, Subbaraman R, Tripkovic D, Karapetrov G, Stamenkovic VR, Pejovnik S, Marković NM (2010) Nat Mater 9(12):998–1003